RSC Advances

PAPER

View Article Online
View Journal | View Issue

Cite this: *RSC Adv.*, 2024, **14**, 11524

Highly emissive blue graphene quantum dots with excitation-independent emission *via* ultrafast liquid-phase photoreduction†

Jae-Won Lee,[ab] Ji Hye Kwak,[c] Juhee Kim,[b] Yoon-Kwan Jang,[d] Joong Tark Han,[b] Tae-Jin Kim,[d] Kyong-Soo Hong,[e] Hee Jin Jeong*[b] and Imjeong H.-S. Yang*[a]

Received 13th February 2024
Accepted 2nd April 2024

DOI: 10.1039/d4ra01113a

rsc.li/rsc-advances

Graphene oxide quantum dots (GOQDs) are promising candidates for biomedical applications since they have lower toxicity and higher biocompatibility than traditional semiconductor quantum dots. However, oxygen functional groups such as epoxy and hydroxyl groups usually induce nonradiative relaxation, which leads to GOQDs exhibiting nonemissive properties. For the enhancement of the emission efficiency of GOQDs, the number of nonradiative relaxation sites should be reduced. This paper reports the synthesis of highly luminescent reduced GOQDs prepared by liquid-phase photoreduction (LPP-rGOQDs). First, GOQDs was fabricated from single-walled carbon nanotubes through chlorate-based oxidation and separation after acoustic cavitation. Subsequently, LPP-rGOQDs were obtained by liquid-phase photoreduction of the GOQD suspension under intense pulsed light irradiation. Liquid-phase photoreduction selectively reduced epoxy groups present on the basal plane of GOQDs, and hydrogenated the basal plane without removal of carbonyl and carboxyl groups at the edges of the GOQDs. Such selective removal of oxidative functional groups was used to control the reduction degree of GOQDs, closely related to their optical properties. The optimized LPP-rGOQDs were bright blue in color and showed quantum yields up to about 19.7%, which was 10 times the quantum yield of GOQDs. Furthermore, the LPP-rGOQDs were utilized to image a human embryonic kidney (HEK293A), and a low cytotoxicity level and satisfactory cell imaging performance were observed.

1. Introduction

Among carbon-based nanomaterials, graphene oxide quantum dots (GOQDs) are considered to have a high potential for use in the fields of bioimaging, biomedicine, biosensing, and optoelectronics, owing to their exceptional properties such as stable photoluminescence (PL), pronounced quantum confinement effect, high chemical stability, and low toxicity.[1–10] Generally, subjecting bulk carbon sources, such as graphite nanoparticles, single-walled carbon nanotubes (SWCNTs), and multi-walled carbon nanotubes, to strong oxidation and exfoliation yields GOQDs, which contain different oxygen functional groups, such as epoxy, hydroxyl, carbonyl, and carboxyl groups.[11–17] These oxygen functional groups can be removed through reduction processes to obtain partially or fully reduced GOQDs (rGOQDs).[18–21] This removal possibility offers interesting perspectives in the field of optical physics, optical engineering, and optoelectronics. Many researchers have studied the synthesis of GOQDs and rGOQDs and their optical properties because of the quantum confinement effects, surface/edge states, oxygenated groups, and the synergistic effect of all these factors.[22–26] In general, the fundamental mechanisms responsible for the PL properties of GOQDs suggest that the photoluminescence emission originates from sp^2 carbon domains localized by the sp^3-bonded carbon bound to oxygen.[14] The carbon–oxygen bonds disrupt the extended sp^2 conjugated network and localized sp^2 carbon domains in which π-electrons are confined; consequently, the bandgap becomes finite, which causes fluorescence because of electron–hole radiative recombination (the so-called intrinsic emission). The oxygen-bound sp^3-bonded carbon can be regarded as a fluorophore, showing long-wavelength fluorescence (the so-called extrinsic emission).[27,28] The extrinsic emission from the oxidized sp^3 site can

[a]*Department of Physics, Pusan National University, Busan 46241, South Korea. E-mail: ijyang@pusan.ac.kr*
[b]*Nano Hybrid Technology Research Center, Creative and Fundamental Research Division, Korea Electrotechnology Research Institute (KERI), Changwon 51543, Republic of Korea. E-mail: wavicle11@keri.re.kr*
[c]*Electrical Environment Research Center, Power Grid Research Division, Korea Electrotechnology Research Institute (KERI), Changwon 51543, Republic of Korea*
[d]*Department of Biological Sciences, Pusan National University, Busan 46241, South Korea*
[e]*Busan Center, Korea Basic Science Institute (KBSI), Busan 46742, South Korea*

† Electronic supplementary information (ESI) available: Schematic illustration of the preparation of GOQDs, TEM image of GOQDs and LPP-rGOQDs, XPS spectra of SWCNT, Ox-SWCNT, GOQDs, and LPP-rGOQDs, photograph of xenon flash lamp system, PL spectrum of GOQDs and LPP-rGOQDs, photograph of GOQDs and LPP-rGOQDs suspension. See DOI: https://doi.org/10.1039/d4ra01113a

be easily tuned by removing some surrounding oxygen functional groups.

The process of deoxygenation of GOQDs, which is used for producing rGOQDs, significantly influences the optical properties of the rGOQDs produced. In particular, oxygen functional groups such as epoxy and hydroxyl groups introduced on the basal plane of GOQDs during the oxidation process render the charge transfer process much more complex and are a major factor inducing nonradiative relaxation, which can reduce the fluorescence emission efficiency. The emission efficiency can be significantly enhanced by reducing nonradiative relaxation, which can be achieved by removing the epoxy and hydroxyl groups through reduction processes. The oxygen functional groups of GOQDs can be chemically removed using reducing agents (*e.g.*, hydrazine, vitamin C, sulfuric acid, and sodium hydroxide), thermally removed by heating the GOQDs (direct or microwave-induced heating) to a high temperature, or optically removed. Recently, many researchers have studied the optical properties of rGOQDs prepared through various reduction methods. Zhu *et al.* reported the successful fabrication of high-efficiency blue-luminescence graphene quantum dots (GQDs) through the chemical reduction of green-luminescence GQDs, and Liu *et al.* synthesized rGOQDs with tunable PL by thermally reducing GOQDs at different temperatures.[23,29] However, although chemical and thermal treatments are popular GOQD reduction methods, they are very slow and hazardous. In stark contrast, photoreduction processes involving a xenon (Xe) flash lamp, IR light, or laser beams are straightforward and do not require hazardous reducing agents or high temperatures. For example, intense pulsed light (IPL) in a broad wavelength spectrum can be obtained with a Xe flash lamp, and it is commonly used for reducing oxidized nanocarbons; the duration of the reduction process is a few milliseconds.[30–36] Notably, the oxygen atoms of epoxy groups located on the basal plane can be selectively dissociated through photoexcitation because of the antibonding character of the photoexcited state.[37] This suggests that epoxy groups related to nonradiative relaxation can be effectively removed through photoreduction, which implies that rGOQDs with specific functional groups for optoelectronic applications can be obtained through photoreduction.

In this study, GOQDs were produced through chlorate-based oxidation of SWCNTs *via* a highly effective kneading process by varying the amount of oxidant and reaction time. Rapid and high-efficiency oxidation of SWCNTs yielded GOQDs with an average lateral diameter of 3.37 nm and a size deviation of ±0.1 nm. Furthermore, a novel pathway was developed for the ultrafast photoreduction of colloidal GOQDs at a low temperature and under ambient conditions through irradiation with continuous-wave Xe flashlight as the IPL source. The number of epoxy groups involved in nonradiative relaxation in GOQDs can be successfully controlled by controlling the photoreduction conditions. The final product of GOQDs through liquid-phase photoreduction exhibits excitation-independent emission with higher photoluminescence quantum yield compared to GOQDs before liquid-phase photoreduction. Interestingly, direct heating of GOQDs through IPL irradiation instantaneously generates a very large amount of heat, which triggers the dissociation of adjacent solvent molecules to produce radicals or active species (*i.e.*, e_{aq}^-, $OH^\bullet$, $H^\bullet$, H_3O^+, and OH^-). In particular, it was found that the hydrogen radical combines with the dangling bonds located on the basal plane of the GOQDs produced through liquid-phase photoreduction (hereafter referred to by the abbreviation LPP-rGOQDs) to form sp^3 C–H bonds, which reduced the number of defect states associated with the dangling bonds. Finally, the LPP-rGOQDs were utilized as fluorescent labels for imaging biological cells. Notably, highly sensitive imaging without significant cytotoxicity was observed even at a high LPP-rGOQDs concentration, which reveals that the rGOQDs have the potential to be used in the fields of bioimaging, biomedicine, and optoelectronics.

2. Experimental

2.1 Materials

SWCNTs powder (TUBALL, 75% purity) synthesized using the chemical vapor deposition method was obtained from OCSiAl. Fuming nitric acid was purchased from Tokyo Chemical Industry, and $NaClO_3$ was purchased from Samchun Chemicals. All chemicals were used without further purification.

2.2 Liquid-phase photoreduction of GOQDs

IPL treatment of GOQDs suspension was carried out at room temperature in the air. Intense light with a pulse frequency of 100 Hz was produced from a Xenon lamp equipped in a UXF-S/K100-145-DWC (Unilam Co., Korea), in which the effective range was 150 × 150 mm with uniformity of 97.5%. LPP-rGOQDs suspension was fabricated from the GOQDs suspension. First, 30 ml of GOQDs suspension was added into a 100 ml of quartz vial. Second, the GOQDs suspension was treated by multiple-pulses IPL with a total exposure time between 20 ms to 100 ms by the same output voltage within an exposure time of 1 ms. At last, The LPP-rGOQDs suspension was centrifuged at 15,000 rpm for 30 min to remove the sediment. The LPP-rGOQDs suspension were marked as LPP20-rGOQDs, LPP40-rGOQDs, LPP60-rGOQDs, and LPP100-rGOQDs, respectively, according to the IPL total exposure time.

2.3 Cell culture

Human embryonic kidney (HEK293A) cells were obtained from Dr Jihye Seong (KIST) and cultured in Dulbecco's modified Eagle's medium (DMEM, CM002-050, GenDEPOT) supplemented with 10% fetal bovine serum (FBS, SH30084.03, HyClone), 100 U ml^{-1} penicillin and 100 μg ml^{-1} streptomycin (CA005-010, GenDEPOT). The cells were cultured in a humidified incubator of 95% air and 5% CO_2 at 37 °C.

2.4 Cell viability assay

Cell viability was detected using the Cellrix® Viability Assay Kit (B1007-500, Cellrix). HEK293A cells (5×10^3 cells per well) were seeded in the 96-well plates. After culturing for 24 h, the medium was removed, and the cells were exposed to different concentrations of molecular water (W4502, Sigma) and LPP100-

rGOQDs. After 24 h of incubation, the Cellrix® Viability Assay Kit was added and incubated additional 1 h. The absorbance was measured at a test wavelength of 450 nm and a reference wavelength of 600 nm by the GloMax™ Multi Reader (9301-010, Promega).

2.5 Characterization

Absorption spectra are measured at room temperature by using a UV-Visible spectrometer (Cary 5000, Agilent). Photoluminescence (PL) spectra are acquired upon excitation by using a xenon lamp (LabRAM HR-800 UV-Visible-NIR). The temperature of the GOQDs during IPL treatment was measured by an infrared sensor (IGA 740-LO, LumaSense Technologies GmbH, Germany). The oxidation levels of the GOQDs and LPP-rGOQDs were measured by X-ray photoelectron spectroscopy (XPS) using a Multilab2000 (Thermo VG scientific Inc). Raman spectra were measured using a Raman spectrometer (NTEGRA SPECTRA, NT-MDT Spectrum Instrument, Russia) with an excitation wavelength of 532 nm. Transmission electron microscope (TEM) images and energy dispersive spectrometer (EDS) data were recorded on an electron microscope (TECNAI F20, FEI/Philips, USA) operating at 200 kV. The intense light energies were measured using a pulse energy sensor (L40(150)A, OPHIR) and energy meter (Vega, OPHIR). Time-resolved PL spectra are measured with time-correlated single photon counting (TCSPC) through time to amplitude conversion by using a pulsed laser diode (HORIBA SCIENTIFIC). Fourier transform infrared spectroscopy (FTIR) were measured using a FT/IR-4X FTIR spectrometer (Jasco Inc.). Zeta potential measurements were performed on a Malvern Zetasizer Nano series Nano ZS.

3. Results and discussion

3.1 Preparation of LPP-rGOQDs

GOQDs were prepared by a top-down approach starting from a chlorate-based oxidation of SWCNTs *via* a kneading process, as described in our previous report.[38] The mechanical activation of semi solid-state mixing by kneading causes strong chemical interaction between SWCNTs and oxidant molecules, resulting in the fast oxidation and high oxidation efficiency of SWCNTs (Fig. S1a†). The oxidation level of SWCNTs critically depends on the ratio of SWCNTs/$NaClO_3$ and reaction time. The amount of oxygen functional groups and corresponding structural defects of the SWCNTs were gradually increased with increasing the oxidant contents and reaction time. Considering the fact that the GOQDs could be effectively synthesized by splitting the oxidized SWCNTs having defective wall structures, in this study, we deliberately used a specific experimental condition of SWCNT/$NaClO_3$ weight ratio of 1 : 10 and reaction time of 5 h, which is much harsh condition compared with our previous results about the rational oxidation for obtaining thermodynamically stable SWCNTs dispersions in water. Therefore, this specific oxidation condition leads to cap opening and unzipping of the SWCNTs more efficiently, and finally cutting into tiny graphene pieces after a consecutive ultrasonication treatment. As a result, the tubular structure of SWCNTs was almost destroyed, forming abundant GOQDs (Fig. S1a†). Transmission electron microscopy (TEM) micrographs in Fig. S1b† indicate that the kneading-oxidation process makes the structure of SWCNTs change greatly because of the introduction of oxidative groups and defects. These results are in good agreement with oxidation concepts illustrated in Fig. S1a† and X-ray photoelectron spectroscopy (XPS) spectrum shown in Fig. S2.† Fig. S1c and d† shows TEM micrographs of GOQDs prepared by kneading–oxidation process and following ultrasonication treatment. The corresponding normalized particle size distribution histograms shown in the inset of Fig. S1c† revealed that GOQDs have an average lateral diameter of 3.37 nm with a size deviation of ±0.1 nm. The high-resolution TEM micrographs in the inset of Fig. S1d† clearly show the crystalline nature of the GOQDs. The lattice parameter was measured to be 0.21 nm, corresponding to the {1100} lattice fringes of graphene.[39]

The physicochemical and optical properties of the GOQDs suspension were systematically investigated by controlling the oxygen functionalities through IPL as a heat source for ultrafast liquid-phase photoreduction. Fig. 1a illustrates the millisecond-scale optical annealing procedures in which LPP-rGOQDs were prepared from GOQDs. The GOQDs suspension was firstly placed at the center of the IPL sample stage and exposed to multiple-pulse IPL generated by the Xe flash lamp (Fig. S3a†). White light with a broad wavelength ranging from 350 nm to 800 nm was emitted from the Xe flash lamp as shown in Fig. S3b.† During the IPL irradiation, the light absorption by the GOQDs resulted in a great temperature increase owing to the photothermal effect originated from high localized surface plasmon density, which enabled the removal of oxygen functional groups in the GOQDs and dissociation of adjacent solvent molecules to produce radicals or active species (*i.e.*, e_{aq}^-, $OH^\bullet$, $H^\bullet$, H_3O^+, and OH^-) (Fig. 1a-i). The presence of hydrogen radical in the solvent favors the removal of oxygen functional groups *via* consecutive hydrogenation reactions. Also, these reactions also seem to introduce sp^3 C–H bonds due to the hydrogen radical combines with the dangling bonds created after removing oxygen functional groups located in the basal planes of GOQDs through liquid-phase photoreduction (Fig. 1a-ii). Fig. 1b represents the temperature profiles of the GOQDs in powder form irradiated with multiple pulses of an energy density of 4 J cm^{-2} at a pulse repetition rate of 30 Hz. We could hardly observe the significant heat accumulation on the samples because the time interval (33 ms) between two pulses provides sufficient time for heat dissipation at this pulse repetition rate of 30 Hz. Furthermore, very rapid temperature increase in every pulse shot was clearly observed owing to the direct conversion of the absorbed light into heat. Therefore, the effective photoreduction of GOQDs could be possible with the appropriate IPL irradiation. For detailed examination of the rapid heating and cooling, the temperature profile of the sample is measured during IPL irradiation with a single shot with an exposure time of 1 ms as shown in Fig. 1c. Immediately on IPL irradiation, the temperature was suddenly raised owing to light-absorption-induced rapid heating of the GOQDs.

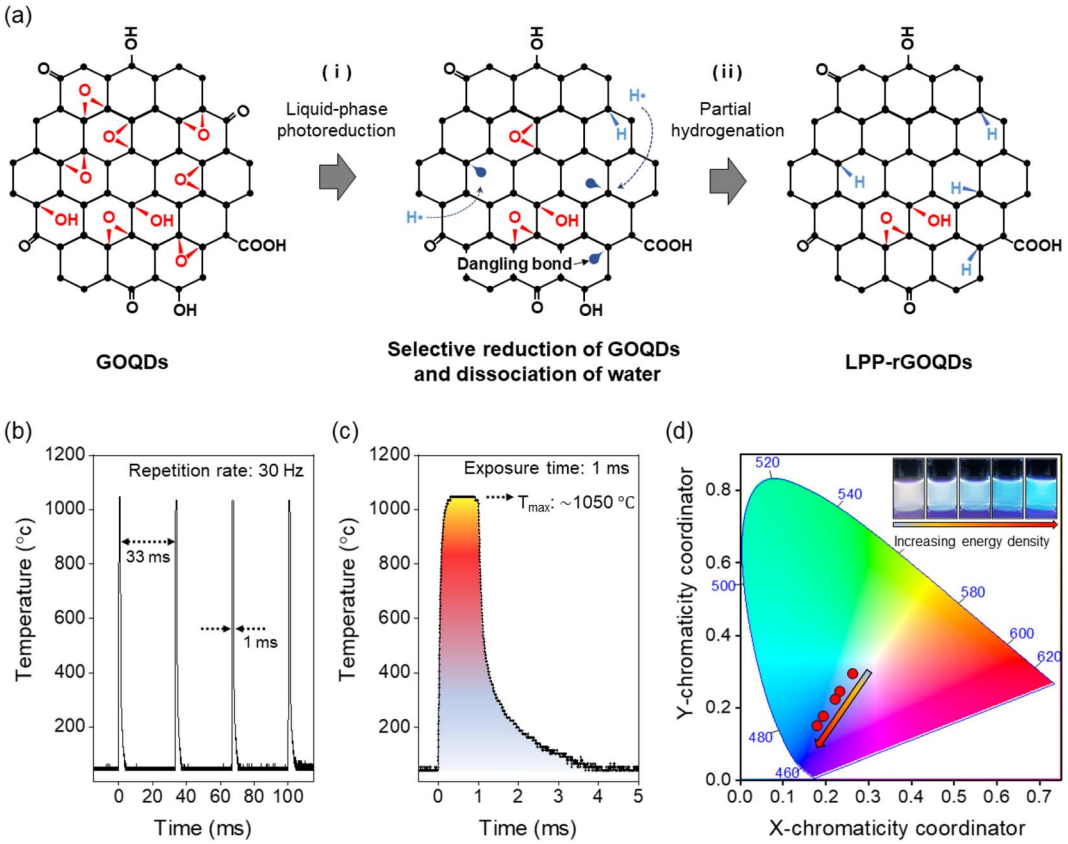

Fig. 1 (a) Schematic illustration for the synthesis of liquid-phase photoreduced GOQDs. (b) *In situ* monitoring of temperature change of GOQDs during multiple-pulses IPL irradiation (exposure time: 1 ms, repetition rate: 30 Hz). (c) Temperature–time profile of GOQDs for single pulses at pulse energy of 4 J cm^{-2}. (d) CIE 1931 chromaticity coordinates of GOQDs and LPP20 to LPP100-rGOQDs suspension, excited at 320 nm. (Fluorescence image shows a photograph of GOQDs suspension exposed to multiple-pulse IPL of increasing total exposure time from left to right).

Indeed, the temperature reaches a maximum value of 1050 °C within only 0.3 ms and lasts until the rest of the pulse duration. Then, the GOQDs were quickly cooled to below 50 °C. As shown in Fig. S4,† the temperature ramp rates for light-absorption-induced ultrafast heating and cooling were calculated to be 3.5×10^6 °C s^{-1} and 2.5×10^5 °C s^{-1}, respectively, which are approximately 1.8×10^6 times faster than that in a conventional thermal treatment.[29] The Commission International de l' ' clairage (CIE) 1931 chromaticity coordinates were calculated for the GOQDs and LPP20 to LPP100-rGOQDs suspensions under 320 nm excitation wavelength (Fig. 1d). The arrow in the diagram shows the change in the CIE coordinates as the IPL exposure time increases up to 100 ms. In the case of GOQDs suspension, CIE parameters were $x = 0.26$, $y = 0.29$, which are quite close to those of pure white-light emission (0.33, 0.33). The corresponding CIE parameters of LPP100-rGOQDs were located at (0.18, 0.15), which belonged to the pure blue emission.

3.2 Characterization of LPP-rGOQDs

Deoxygenation and hydrogenation of samples by liquid-phase photoreduction were investigated by analyzing the specific functional groups of GOQDs and LPP100-rGOQDs using Fourier transform infrared (FTIR) (Fig. 2a). As shown in FTIR results, two bands related to stretching vibrations of C–H bonds at 2899 and 2973 cm^{-1} characteristics were clearly observed after liquid-phase photoreduction, providing conclusive evidence for the hydrogenation of LPP100-rGOQDs. In addition, it was confirmed that all major oxygen functional groups were present despite liquid-phase photoreduction with harsh conditions. The peaks for C–O stretching, C–O–C (epoxy), C–OH groups, C=C (sp^2 of aromatic ring), and C=O stretching at 1056, 1226, 1390, 1636, and 1730 cm^{-1}, respectively, were still observed after liquid-phase photoreduction. The crystal structure of the GOQDs and LPP-rGOQDs was investigated by the X-ray diffraction (XRD) and Raman spectroscopy. Fig. S5† presents the XRD patterns of the GOQDs and LPP100-rGOQDs. The diffraction peaks of the GOQDs and LPP100-rGOQDs are centered at $2\theta = 21.72°$ and 22.57° corresponding to the (002) plane with a *d*-spacing of 0.409 nm and 0.393 nm. Although the peaks are quite broad compared to that of graphite, this is general behavior in nanoscale size of the graphene QDs with only few layers of graphene sheets.[40] Fig. 2b shows the Raman spectra of the GOQDs and LPP20 to LPP100-rGOQDs. The Raman spectrum of each sample exhibits two main characteristics peaks; the G mode in the Raman spectrum is associated with an in-plane

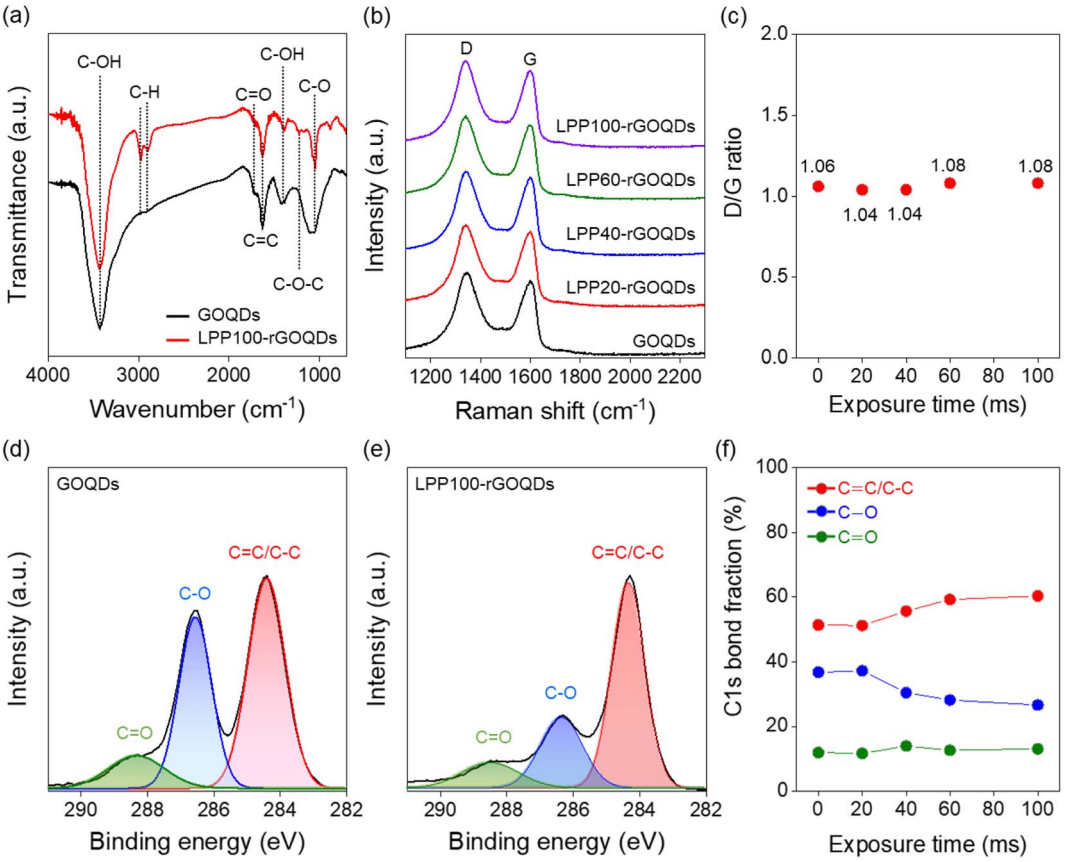

Fig. 2 (a) FTIR spectroscopy of GOQDs and LPP100-rGOQDs. (b) Raman spectra of GOQDs and LPP20 to LPP100-rGOQDs. (c) Ratio of the intensities of D and G bands (I_D/I_G). High-resolution C1s XPS spectra of (d) GOQDs and (e) LPP100-rGOQDs. (f) The evolution of C=C, C–O, and C=O bonds as a function of exposure time.

vibrational mode (approximately 1598.22 cm^{-1}) involving the sp^2 carbon atoms. The D mode (approximately 1339.94 cm^{-1}) is caused by disorder states such as structural defects and oxygen functional groups. Hence, the intensity ratios of the D and G bands can be used to determine the level of disorder in the carbon materials.[41,42] Interestingly, the I_D/I_G ratio is not significantly changed at all samples (Fig. 2c). Considering the results of XPS (Fig. 2d–f) and EDS (Fig. S6c†) about deoxygenation of GOQDs by the IPL irradiation, the intensity of D peak should be gradually decreased. Therefore, this anomalous behavior was assumed to be the results of hydrogenation of the LPP-rGOQDs during the liquid-phase photothermal process. Hydrogenation for the LPP-rGOQDs was clearly confirmed by the FTIR results as shown in Fig. 2a.[36]

Evidence of the deoxygenation of the GOQDs by liquid-phase photoreduction was investigated with XPS, as shown in Fig. 2d and e, the C1s signals can be deconvoluted into three main peaks of sp^2 carbon (C=C, 284.5 eV), epoxy groups (C–O, 286.5 eV), and carbonyl groups (C=O, 288.2 eV) in both GOQDs and LPP100-rGOQDs.[31,32] The relative intensity of the epoxy groups of LPP100-rGOQDs decreases dramatically, compared to that of GOQDs, whereas carbonyl groups was almost unchanged. This was also confirmed by the XPS results for the LPP20-, LPP40-, and LPP60-rGOQDs as shown in Fig. S7.† As demonstrated in Fig. 2f, the C1s chemical bond fraction can be defined as the integrated peak areas of the sp^2 carbon, epoxy groups (C–O), and carbonyl groups (C=O) calculated from the XPS results. The initial fraction of the carbon atoms that are sp^2-bonded in the GOQDs is approximately 51.3%. This fraction gradually increases with the IPL exposure time and reaches a maximum of approximately 60.3% in the LPP100-rGOQDs. On the other hand, the fraction of epoxy groups decreases from 36.8 to 26.6%, suggesting that most of the oxygen functional groups attached on the basal plane of LPP100-rGOQDs can be readily removed.[43] It is worth noting that there are no clear change in the fraction of carbonyl groups. The carbonyl groups functionalized primarily on the edge parts of the GOQDs are generally known to be most stable one among the oxygen-related groups, thus they are hardly removed even in this relatively strong IPL irradiation condition.

3.3 Optical properties of LPP-rGOQDs

The tuning of the optical properties of the GOQD suspension by varying the IPL exposure time was studied with UV-Vis absorption spectra and PL spectra, as shown in Fig. 3a and b. The UV-Vis absorption spectrum of each sample shows a strong absorption peak in the UV region, which originates from the π–π* transition of the aromatic sp^2 domain (Fig. 3a).[1] The

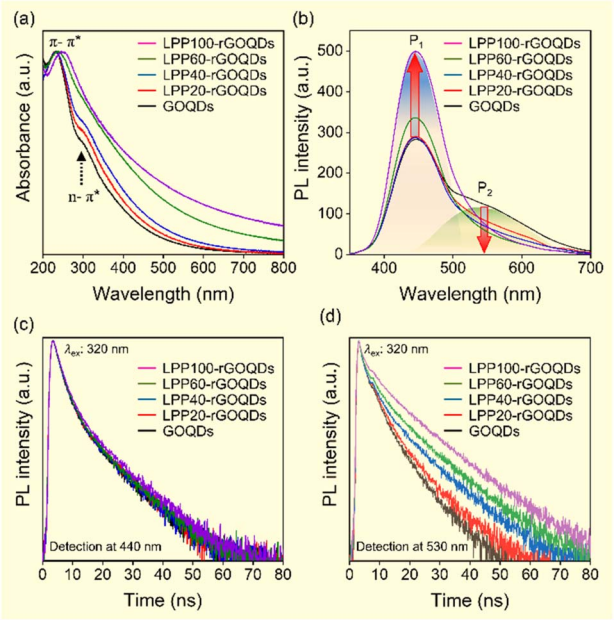

Fig. 3 (a) The UV-Vis absorption spectra of GOQDs and LPP20 to LPP100-rGOQDs suspension. (b) PL spectra of GOQDs and LPP20 to LPP100-rGOQDs suspension excited at 320 nm. Time-resolved photoluminescence spectra of GOQDs and LPP20 to LPP100-rGOQDs suspension monitored at (c) 440 nm and (d) 530 nm.

absorption peak undergoes a redshift from 232 to 245 nm upon the liquid-phase photoreduction of the GOQDs. This shift is due to the restoration of sp^2 conjugated structure and increasing electron concentration.[44] The broad shoulder at 290–305 nm corresponds to the n–π* transition of oxygen functional groups.[45] The deoxygenation is reconfirmed by the disappearance of the n–π* transition in the UV-Vis absorption spectra when the IPL exposure time was more than 60 ms. Fig. 3b and S8a† show the corresponding PL spectra and normalized PL spectra of the GOQDs and LPP20 to LPP100-rGOQDs suspensions, which were deconvoluted into two Gaussian fitting peaks: P_1 (the so-called intrinsic emission) and P_2 (the so-called extrinsic emission) centered at different wavelengths. The PL of the GOQDs suspension is dominated by the P_1 peak centered at approximately 445 nm and the broad P_2 emission peak centered at approximately 530 nm. The peak position of P_2 shifts from 530 nm for the GOQDs suspension to 500 nm after the IPL irradiation for 100 ms. By contrast, the peak position of P_1 slightly shifts to shorter wavelengths. The LPP100-rGOQDs suspension exhibits a strong emission peak centered at approximately 440 nm, which is accompanied by a very weak P_2 emission peak. The rate of increase of the P_1 intensity of LPP100-rGOQDs suspension was nearly two times greater than the GOQDs suspension. In addition, the LPP100-rGOQDs were bright blue in color and showed quantum yields up to about 19.7%, which was 10 times the quantum yield of GOQDs (Table. S1†). In general, the blue emission peak (approximately 440 nm) mainly results from the small isolated sp^2 carbon domains, while the long-wavelength emission peak is related to oxygen functional groups.[17,27,28] Interestingly, the photodissociation of epoxy groups in the XPS study strongly correlates with the change in P_1 and P_2 intensity. As IPL exposure time increases, the incremental photoreduction in epoxy groups leads to a gradual decrease in the P_2 emission peak and the corresponding increase in the P_1 emission peak. This can be due to the eliminated epoxy groups on the basal plane of GOQDs, which decreased the oxygen-related defect states within the π–π* gaps and increased the number of newly formed, small, isolated sp^2 carbon domains.[18,46] The full width at half maximum (FWHM) values of P_1 and P_2 of the GOQDs and LPP20 to LPP100-rGOQDs suspension are shown in Fig. S9a.† The FWHM values of the P_1 and P_2 emission peaks can reflect the distributions of the sp^2 carbon domains and oxygen functional groups of the GOQD or LPP20 to LPP100-rGOQDs suspensions.[33] The FWHM of the P_1 emission peak exhibits a narrow size dispersion, which implies the distribution of small isolated sp^2 carbon domains within the GOQDs and LPP20 to LPP100-rGOQDs suspensions. Therefore, as the reduction of GOQDs proceeds, the size of the sp^2 carbon domains does not increase after removal of oxygen in photoreduction. By contrast, the difference in the FWHM values of the P_2 emission peaks of the GOQDs and LPP20 to LPP100-rGOQDs suspensions is approximately 50 nm, which implies the existence of non-radiative trap states associated with the different amounts of oxygen functional groups of the GOQDs and LPP20 to LPP100-rGOQDs suspensions. The integrated area of the P_2 emission peak decreases from 58 to 28% after liquid-phase photoreduction, while that of the P_1 emission peak increases from 42 to 72% (Fig. S8b–f†). Moreover, the P_1/P_2 ratio of each sample as a function of the exposure time is shown in Fig. S9b,† which demonstrates a strong correlation with the increased C/O atomic ratio calculated from the XPS results. Accordingly, the evolution of the PL emission peak mainly arises from the varying P_1 to P_2 emission intensity ratios, which results from the increasing number of sp^2 carbon atoms with the removal of the oxygen functional groups. In order to prove the liquid-phase photoreduction of the GOQDs, we prepared the suspensions of the GOQDs and LPP20 to LPP100-rGOQDs under daylight and UV light (wavelength of 320 nm) as shown in the Fig. S10.† The brown solution (GOQDs) gradually becomes colorless under daylight with increasing IPL exposure time.

Moreover, the yellow-white emission (GOQDs) turns to light blue and bright blue under the excitation of a UV lamp, depending on the degree of liquid-phase photoreduction of LPP100-rGOQDs are seen to be excitation-independent, while those of GOQDs clearly shift toward longer wavelengths with the increase of excitation wavelength.

3.4 Time-resolved photoluminescence analysis

In order to understand the recombination dynamic mechanism of GOQDs and LPP20 to LPP100-rGOQDs, we performed time-resolved PL (TRPL) experiments from main emission peaks of 440 nm and 530 nm corresponding to recombination of intrinsic states and extrinsic states, respectively (Fig. 3c and d). Table S2† depicts the values obtained by fitting values of parameters. The PL decay curves of each sample were fitted by a double exponential fitting function:

$$I(t) = A_1 \exp\left(-\frac{t}{\tau_1}\right) + A_2 \exp\left(-\frac{t}{\tau_2}\right) \quad (1)$$

where τ_1 and τ_2 indicate the lifetimes of two different radiative decay processes ($\tau_1 < \tau_2$), and A_i is an amplitude of decay process with a lifetime τ_i. Here, τ_1 is the radiative lifetime by the initially populated e-h recombination in QDs. τ_2 of the slower decay represents the radiative process related to the surface defect state. The surface defect state-trapped carriers get the energy support by interaction with vibrational modes and recombine to relax energy radiatively, which results in a slower energy decay process compared with the initially populated e-h recombination process. In addition, we have calculated the average PL lifetime τ_{ave} as:

$$\tau_{ave} = \frac{A_1\tau_1^2 + A_2\tau_2^2}{A_1\tau_1 + A_2\tau_2} \quad (2)$$

As shown in Fig. 3c, 440 nm TRPL lifetime shows the slightly slower decay curves with the increasing of the IPL exposure time. The lifetimes for GOQDs exhibit an initial fast decay of 2.36 ns timescale followed by a tail of 10.12 ns, and those for LPP100-rGQDs are 2.8 ns and 14.46 ns timescales. The obtained lifetimes are attributed to the intrinsic state of the initially excited carbogenic core. Therefore, the LPP100-rGOQDs a long lifetime compared to the GOQDs due to a gradual increase in the charge carrier associated with the intrinsic state. In addition, with increasing the IPL exposure time, the average lifetime was also prolonged. The average lifetime for the intrinsic state gradually increased from 5.55 ns to 7.33 ns with IPL exposure time, which is closely related to the LPP100-rGOQDs with improved intrinsic emission (440 nm; blue emission) after liquid-phase photoreduction. Meanwhile, the 530 nm TRPL lifetime associated with extrinsic state evidently increases with IPL exposure time (Fig. 3d). This result is ascribed to the reduced defect states resulting from photoreduction of oxygen functional groups in GOQDs. In general, surface defect state-related non-radiative recombination quenches the PL lifetime in the QDs.[47] As expected the lifetime is susceptible to oxygen functional groups-related to surface defect, so the average lifetime in GOQDs increased after liquid-phase photoreduction.

3.5 Excitation-related emission mechanism

A clear insight into the PL variation during the oxygen reduction of GOQDs is crucial for understanding the excitation-related emission processes. Fig. 4a, b, and S11a–c† shows the PL spectra of GOQDs and LPP20 to LPP100-rGOQDs suspensions for different excitation wavelengths. The excitation–emission process demonstrates that the PL characteristics of the GOQDs depend on the excitation-increased. The reason for the redshift is that the defect state emission originates from the oxygen functional groups in the GOQDs, which have different energy levels and thereby lead to a series of surface trap states.[43] However, the maximal emission peak of the LPP100-rGOQDs does not undergo this spectral shift. Because they do not possess oxygen functional groups, the LPP100-rGOQDs do not exhibit excitation dependence. Fig. S11d† shows the maximal

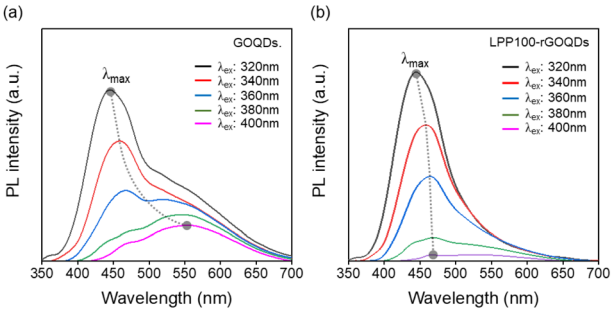

Fig. 4 PL spectra of (a) GOQDs and (b) LPP100-rGOQDs suspension at various excitation wavelength. The excitation wavelength was varied from 320 nm to 400 nm with a fixed increment of 20 nm.

emission peak of GOQDs and LPP100-rGOQDs suspensions for different excitation wavelengths. In agreement with the above discussion, the maximal emission peaks of LPP100-rGOQDs are seen to be excitation-independent, while those of GOQDs clearly shift toward longer wavelengths with the increase of excitation wavelength.

3.6 Cellular imaging and cytotoxicity study

To investigate the biological applicability, we treated the LPP100-rGOQDs to HEK293A cells. LPP100-rGOQDs had a zeta potential of −29 mV (Fig. S12†). HEK293A cells were seeded in a confocal microscopy dish and incubated with LPP100-rGOQDs at 37 °C for 24 h. After treatment of LPP100-rGOQDs, we found that the cells absorbed the LPP100-rGOQDs without any other treatments (Fig. 5a). Confocal imaging was performed on an Zeiss LSM-800 laser scanning microscope with a 40× C-Apo objective/numerical aperture (NA) 1.20. Laser-excitation wavelength were 488 nm with 2% laser power. The absorbed LPP100-rGOQDs were located along the edge of the cells, however, there was no significant uptake difference between the concentration. Next, to assess the cytotoxicity of LPP100-rGOQDs on cells, we analyzed cell viability (Fig. 5b). The data showed that the LPP100-rGOQDs have no cytotoxic effects on

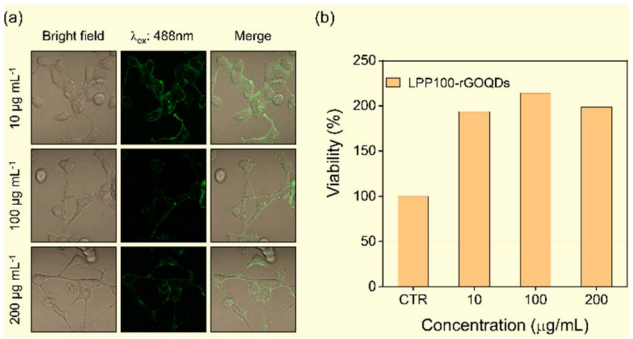

Fig. 5 Confocal fluorescence images of HEK293A cells incubated with 10 μg mL^{-1}, 100 μg mL^{-1}, and 200 μg mL^{-1} of LPP100-rGOQDs. (a) Cell viability of the HEK293A cells *via* incubation with LPP100-rGOQDs at different concentrations for 24 h. (b) Cell viability using Cellrix® viability assay for HEK293A cells treated with different concentrations of LPP100-rGOQDs.

the cells, even at high concentrations of LPP100-rGOQDs. Together, the results suggest that the LPP100-rGOQDs can be used as a biological sensing application without other mediators or cytotoxic effect.

4. Conclusions

In summary, we have successfully demonstrated the continuous tuning of optical properties in GOQDs through liquid-phase photoreduction with IPL from GOQDs produced by using chlorate-based oxidation of SWCNTs *via* a highly effective kneading process. More specifically, the oxygen functional groups in GOQDs are tuned by controlling the exposure time of the IPL. The optically induced deoxygenation and hydrogenation were probed with XPS and FTIR analysis. The GOQDs suspension has exhibited two main PL emission peaks; One is the sp^2 carbon domain-related emission peak at approximately 445 nm, and the other is an oxygen functionalities-related emission peak at approximately 530 nm. Through the deoxygenation with multiple pulses of IPL, the incremental optical reduction in oxygen functional groups leads to a gradual decrease in the oxygen functional groups-related emission peak and the corresponding increase in the sp^2 carbon domain-related emission peak. The modified optical properties of LPP-rGOQDs leading to varied decay times observed through TRPL measurements also support the premise. Finally, the LPP-rGOQDs are successfully used as fluorescent labels for imaging HEK293A cells. We hope that this work will provide the design of customized GOQDs with tunable PL properties, realizing their potential in the bio-imaging, biomedicine, and optoelectronics areas.

Conflicts of interest

There are no conflicts to declare.

Acknowledgements

This research was supported by Korea Basic Science Institute Grant No. C330320, Busan Metropolitan City, Korea, Grant No. PO2022079, and by the National Research Foundation of Korea (NRF) grant funded by the Korea government (MSIP) (Grant No. 2021R1A2C1004266), and by Primary Research Program (24A01050) of the Korea Electrotechnology Research Institute. H. J. J. was also partially supported by Nano-Convergence Foundation funded by MSIP & MOTIE (Grant No. RS-2023-00257573).

References

1 K. S. Novoselov, A. K. Geim, S. V. Morozov, D. Jiang, Y. Zhang, S. V. Dubonos, I. V. Grigorieva and A. A. Firsov, *Science*, 2004, **306**, 666–669.
2 L. A. Ponomarenko, F. Schedin, M. I. Katsnelson, R. Yang, E. H. Hill, K. S. Novoselov and A. K. Geim, *Science*, 2008, **320**, 356–358.
3 K. A. Ritter and J. W. Lyding, *Nat. Mater.*, 2009, **8**, 235–242.
4 T. Gokus, R. R. Nair, A. Bonetti, M. Bohmler, A. Lombardo, S. K. Novoselov, A. C. Ferrari and A. Hartschuh, *ACS Nano*, 2009, **3**, 3963–3968.
5 D. Pan, J. Zhang, Z. Li and M. Wu, *Adv. Mater.*, 2010, **22**, 734–738.
6 T. F. Yeh, W. L. Huang, C. J. Chung, I. T. Chiang, L. C. Chen, H. Y. Chang, W. C. Su, C. Cheng, S. J. Chen and H. Teng, *J. Phys. Chem. Lett.*, 2013, **7**, 2087–2092.
7 S. H. Jin, D. H. Kim, G. H. Jun, S. H. Hong and S. W. Jeon, *ACS Nano*, 2013, **7**, 1239–1245.
8 X. Qingqing, L. Ruiyi and L. Zaijun, *Anal. Chim. Acta*, 2024, **1292**, 342224.
9 L. Laysandra, D. Kurniawan, C.-L. Wang, W.-H. Chiang and Y.-C. Chiu, *ACS Appl. Mater. Interfaces*, 2021, **13**(50), 60413.
10 N. Yu, H. Peng, H. Xiong, X. Wu, X. Wang, Y. Li and L. Chen, *Microchim. Acta*, 2014, **182**, 2139.
11 Y. Dong, H. Pang, S. Ren, C. Chen, Y. Chi and T. Yu, *Carbon*, 2013, **64**, 245–251.
12 Y. Dong, S. Zhang, L. Shi, Y. Chen, J. Ma, S. Guo, X. Chen and H. Song, *Mater. Chem. Phys.*, 2018, **203**, 125–132.
13 S. Ahirwar, S. Mallick and D. Bahadur, *ACS Omega*, 2017, **2**, 8343–8353.
14 Y. Sun, S. Wang, C. Li, P. Luo, L. Tao, Y. Wei and G. Shi, *Phys. Chem. Chem. Phys.*, 2013, **15**, 9907–9913.
15 B. Liu, J. Xie, H. Ma, X. Zhang, Y. Pan, J. Lv, H. Ge, N. Ren, H. Su, X. Xie, L. Huang and W. Huang, *Small*, 2017, **13**, 1601001.
16 S. Kapoor, A. Jha, H. Ahmad and S. S. Islam, *ACS Omega*, 2020, **5**, 18831–18841.
17 F. Liu, M. H. Jang, H. D. Ha, J. H. Kim, Y. H. Cho and T. S. Seo, *Adv. Mater.*, 2013, **25**, 3657–3662.
18 M. H. Jang, H. D. Ha, E. S. Lee, F. Liu, Y. H. Kim, T. S. Seo and Y. H. Cho, *Small*, 2014, **11**, 3773–3781.
19 C. H. Chuang, Y. F. Wang, Y. C. Shao, Y. C. Yeh, D. Y. Wang, C. W. Chen, J. W. Chiou, S. C. Ray, W. F. Pong, L. Zhang, J. F. Zhu and J. H. Guo, *Sci. Rep.*, 2014, **4**, 4525.
20 Y. Zhang, C. Yang, D. Yang, Z. Shao, Y. Hu, J. Chen, L. Yuwen, L. Weng, Z. Luo and L. Wang, *Phys. Chem. Chem. Phys.*, 2018, **20**, 17262–17267.
21 N. Morimoto, T. Kubo and Y. Nishina, *Sci. Rep.*, 2016, **6**, 21715.
22 S. Zhu, Y. Song, X. Zhao, J. Shao, J. Zhang and B. Yang, *Nano Res.*, 2015, **8**, 355–381.
23 S. Zhu, J. Zhang, S. Tang, C. Qiao, L. Wang, H. Wang, X. Liu, B. Li, Y. Li, W. Yu, X. Wang, H. Sun and B. Yang, *Adv. Funct. Mater.*, 2012, **22**, 4732–4740.
24 J. Du, H. Wang, L. Wang, S. Zhu, Y. Song, B. Yang and H. Sun, *J. Mater. Chem. C*, 2016, **4**, 2235–2242.
25 J. Feng, H. Dong, L. Yu and L. Dong, *J. Mater. Chem. C*, 2017, **5**, 5984–5993.
26 G. Rajender and P. K. Giri, *J. Mater. Chem. C*, 2016, **4**, 10852–10865.
27 T.-Fu. Yeh, W.-L. Huang, C.-J. Chung, I.-T. Chiang, L.-C. Chen, H.-Y. Chang, W.-C. Su, C. Cheng, S.-J. Chen and H. Teng, *J. Phys. Chem. Lett.*, 2016, **7**(11), 2087–2092.

28 H. Yoon, Y. H. Chang, S. H. Song, E. S. Lee, S. H. Jin, C. Park, J. Lee, B. H. Kim, H. J. Kang, Y. H. Kim and S. Jeon, *Adv. Mater.*, 2016, **28**, 5255–5261.
29 F. Liu, T. Tang, Q. Feng, M. Li, Y. Liu, N. Tang, W. Zhong and Y. Du, *J. Appl. Phys.*, 2014, **115**, 164307.
30 L. J. Cote, R. Cruz-Silva and J. Huang, *J. Am. Chem. Soc.*, 2009, **131**, 11027–11032.
31 A. Al-Hamry, H. Kang, E. Sowade, V. Dzhagan, R. D. Rodriguez, C. Muller, D. R. T. Zahn, R. R. Baumann and O. Kanoun, *Carbon*, 2016, **102**, 236–244.
32 Z. Wan, S. Wang, B. Haylock, J. Kaur, P. Tanner, D. Thiel, R. Sang, I. S. Cole, X. Li, M. Lobino and Q. Li, *Carbon*, 2016, **141**, 83–91.
33 C. T. Chien, S. S. Li, W. J. Lai, Y. C. Yeh, H. A. Chen, I. S. Chen, L. C. Chen, K. H. Chen, T. Nemoto, S. Isoda, M. Chen, T. Fujita, G. Eda, H. Yamaguchi, M. Chhowalla and C. W. Chen, *Angew. Chem., Int. Ed.*, 2012, **51**, 6662–6666.
34 R. Maiti, A. Midya, C. Narayana and S. K. Ray, *Nanotechnology*, 2014, **25**, 495704.
35 S. R. M. Santiago, T. N. Lin, C. T. Yuan, J. L. Shen, H. Y. Huang and C. A. J. Lin, *Phys. Chem. Chem. Phys.*, 2016, **18**, 22599–22605.
36 Z. Sofer, O. Jankovský, P. Šimek, L. Soferová, D. Sedmidubský and M. Pumera, *Nanoscale*, 2014, **6**, 2153–2160.
37 M. Hada, K. Miyata, S. Ohmura, Y. Arashida, K. Ichiyanagi, I. Katayama, T. Suzuki, W. Chen, S. Mizote, T. Sawa, T. Yokoya, T. Seki, J. Matsuo, T. Tokunaga, C. Itoh, K. Tsuruta, R. Fukaya, S. Nozawa, S. Adachi, J. Takeda, K. Onda, S. Koshihara, Y. Hayashi and Y. Nishina, *ACS Nano*, 2019, **13**, 10103–10112.
38 J. T. Han, J. Y. Cho, J. H. Kim, J. I. Jang, J. S. Kim, H. J. Lee, J. H. Park, J. S. Chae, K. C. Roh, W. Lee, J. Y. Hwang, H. Y. Kim, H. J. Jeong, S. Y. Jeong and G. W. Lee, *Chem. Mater.*, 2019, **31**, 3468–3478.
39 R. V. Nair, R. T. Thomas, V. Sankar, H. Muhammad, M. Dong and S. Pillai, *ACS Omega*, 2017, **2**, 8051–8061.
40 J. Peng, W. Gao, B. K. Gupta, Z. Liu, R. Romero-Aburto, L. Ge, L. Song, L. B. Alemany, X. Zhan, G. Gao, S. A. Vithayathil, B. A. Kaipparettu, A. A. Marti, T. Hayashi, J. J. Zhu and P. M. Ajayan, *Nano Lett.*, 2012, **12**, 844–849.
41 J. Kim and J. S. Suh, *ACS Nano*, 2014, **8**, 4190–4196.
42 J. Wu, P. Wang, F. Wang and Y. Fang, *Nanomaterials*, 2018, **8**, 864.
43 M. Shams, L. M. Guiney, L. Huang, M. Ramesh, X. Yang, M. C. Hersam and I. Chowdhury, *Environ. Sci.: Nano*, 2019, **6**, 2203–2214.
44 M. K. Rabchinskii, A. T. Dideikin, D. A. Kirilenko, M. V. Baidakova, V. V. Shnitov, F. Roth, S. v. Konyakhin, N. A. Besedina, S. I. Pavlov, R. A. Kuricyn, N. M. Lebedeva, P. N. Brunkov and A. Y. Vul, *Sci. Rep.*, 2018, **8**, 14154.
45 P. V. Kumar, N. M. Bardhan, S. Tongay, J. Wu, A. M. Belcher and J. C. Grossman, *Nat. Chem.*, 2014, **6**, 151–158.
46 Z. Gan, H. Xu and Y. Hao, *Nanoscale*, 2016, **8**, 7794–7807.
47 C. Y. Cheng and M. H. Mao, *J. Appl. Phys.*, 2016, **120**, 083103.